Performance of Total Cross Tied Configured Solar Photovoltaic Module Under the Impact of Progressing Shadow Due to Clouds and Self-Shading in Roof Top Installations

Niti Agrawal*‡

*Department of Physics, Shyamlal College, University of Delhi, Delhi-110032, India

‡ Corresponding Author; Niti Agrawal, Tel: +91 9810391961, nitichin@yahoo.co.in

Received: 16.11.2023 Accepted:26.12.2023

Abstract- Partial shading condition (PSC) is a prevalent effective condition which results in huge power loss in solar photovoltaic (SPV) system. The power output of SPV under PSC can be improved by altering the interconnections among PV cells/modules within the PV array i.e., by using different PV array configurations. Many previous studies have assessed the impact of static PSCs on different configurations and found that the total cross tied (TCT) configuration exhibits better performance. However, in real conditions, the shadows are neither static nor uniform. The study on the effect of dynamic or progressing PSCs on TCT configurations has received little attention. In this paper, performance of total cross tied (TCT) PV configuration have been studied under two realistic scenarios of progressing PSCs. These shading conditions are based on the shading due passage of cloud and self-shading in roof top installed PV system. For conducting this study, polycrystalline TCT module has been used. The PV output characteristics have been obtained experimentally using a solar simulator under 6 different shading cases for cloud passage and 9 for progressing horizontal row shading. Values of open circuit voltage, short circuit current, voltage at maximum power point, current at maximum power point, series resistance, maximum power, power loss and efficiency with shadow progression for both the shading scenarios have been obtained. Since the shape of the shadow changes continuously in real life, the obtained results are of significance in understanding the behaviour of TCT configuration over a long period of time under PSCs.

Keywords Partial shading, TCT configuration, progressing shading, sun simulator.

1. Introduction

The world energy demand is increasing colossally and the fossil fuel reserves are getting consumed at an accelerated rate. Consequently, the world is witnessing two serious challenges-energy crisis and adverse impact on the environment. To combat these challenges, global energy system is gradually shifting to the renewable energy sources like solar, biomass, wind and hydro. Solar Photovoltaic (SPV) is gaining popularity globally with technological improvements and rapidly declining costs. In the last five decades, SPV industry has evolved at a remarkable rate. In the last decade (2011-2020) total installed capacity of SPV has increased from 72 GW to 707 GW [1]. By 2050 the cumulative installed capacity of SPV is expected to increase to 8519 GW at a cumulative annual growth rate of 9 percent and generate more than 25 percentage of the total electricity need [2].

In congested urban areas, consumers commonly opt for roof top rack-mounted photovoltaic for electricity generation as it requires lower set-up cost and land requirement [3]. However, when PV modules are installed in the roof top of the building, they encounter a troublesome condition called partial shading condition (PSC) which significantly decreases it's output power [4]. Under PSCs, the solar irradiance falls non-uniformly on PV surface. Partial shading in roof top PV arrays is mainly caused by the shadow created by clouds passage or nearby buildings and inter-row/self-shading [5],[6]. When the PV modules get shaded by the rows of modules placed in the front, it is known as inter-row or self-shading. Practically, such shading cannot be prevented in in limited roof top spaces [7],8]. These scenarios deteriorate the array performance and can causes hotspot formation which results in permanent physical damage to the PV module [9]. The PV output characteristics under PSC also becomes

distorted due to presence of many power peaks [10]. To track the real maximum power point, sophisticated maximum power point tracker (MPPT) are required [11-16] which further increases the system complexity and cost.

Hence, for the mitigation of PS effects, implementation of different array configuration i.e., different interconnections among PV cells/modules within the array is the recent trend [17, 18]. Different PV array configurations such as series (S), parallel (P), series-parallel (SP), bridge linked (BL), honey comb (HC) and total cross tied (TCT) can be implemented. Various studies are present in the literature which have been conducted to investigate the effectiveness of these configuration under PSC [19-25]. These studies have found that under PSCs, TCT configurations suffer lesser power loss and outperforms other configurations. Array reconfiguration techniques for power loss mitigation under PSC are also becoming popular and receiving attention. The reconfiguration strategy aims to optimize the PV yield by dispersing shade over the array to equalize the generated currents by different electrical rows. Reconfiguration can be either static reconfiguration or the dynamic reconfiguration [17]. In static reconfiguration the physical location of the panels is changed keeping the electrical connection same. In dynamic reconfiguration physical location of the panel remains the same but electrical connection are changed. Some of the techniques used for reconfiguration include: mathematical puzzle like Sudoku [26, 27], optimal sudoku [28, 29], magic square puzzle [30], dominance square [31], skyscraper puzzle [32]. However, these techniques also use TCT configuration and reconfigure it using complex network of interconnecting wires. Hence these techniques are not very feasible from the view of practical application owing to the laborious interconnections, increase complexity, and longer length of interconnecting wires which can increasing line losses.

All the above-mentioned studies examined the performance of different configurations generally under the impact of static and even type of shading like row, column or diagonal. However, in real conditions, the shadows are neither static nor uniform. Despite the extensive literature, the effectiveness of configurations under the dynamic shadow received little attention. The impact of varying shadow on TCT configuration is rarely studied. Hence, to

address the above research gap, the performance of TCT configuration is studied experimentally under two realistic scenarios of progressing PSCs which are based on the passage of cloud and self-shading in roof top installed PV system. For this work, a polycrystalline TCT configured module has been used. The output characteristics of TCT module has been obtained using a sun simulator. The performance of the configuration has been studied in terms of the change in the electrical parameters like maximum power, open circuit voltage, short circuit current, voltage at maximum power point, current at maximum power point, series resistance and efficiency with shadow progression. For the purpose of comparison, results are also obtained for a conventional S configured module.

The insight presented in this paper is of great importance in understanding the behaviour of TCT configuration under continuously changing PSCs. This is especially significant for rooftop PV arrays in congested urban environment where it is highly probable that installed PV array is under the influence of dynamic PSCs for large number of days in a year.

2. Modelling of PV Cell and Module

Single diode model of a PV cell, as shown in Fig. 1, is an extensively used model because of its simplicity [33],[34]. This model is also known as five-parameters model. The five parameters of this model are- photo generated current source (I_{phcell}) which depends on the insolation level, reverse saturation current (I_{ocell}) of the inherent p-n diode which is in parallel to the current source, diode ideality factor (n_{cell}), series resistance (R_{scell}) and shunt resistance (R_{shcell}). Using single diode model the current-voltage characteristics of a PV cell (I_{cell}- V_{cell}) can be represented by Eq. (1).

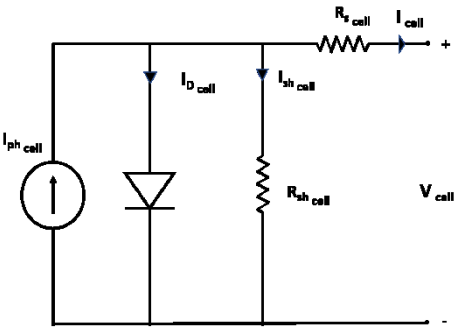

Fig. 1. Single diode model of a PV cell.

$$I_{cell} = I_{ph_{cell}} - I_{o_{cell}} \left[exp\left(\frac{V_{cell}+I_{cell}R_{s_{cell}}}{n_{cell}V_{th}}\right) - 1\right] - \left(\frac{V_{cell}+I_{cell}R_{s_{cell}}}{R_{sh_{cell}}}\right) \quad (1)$$

For a PV module composed of N_p parallel strings, each having N_s cells connected in series, the module current-voltage (I_m - V_m) relationship is expressed by Eq. (2).

$$I_m = N_p \left\{ I_{ph_{cell}} - I_{o\,cell} \left[exp\left(\frac{V_m + I_m R_{s_{cell}} \left(\frac{N_s}{N_p}\right)}{N_s n_{cell} V_{th}} \right) - 1 \right] \right\} - \left(\frac{V_m + I_m R_{s_{cell}} \left(\frac{N_s}{N_p}\right)}{R_{sh_{cell}} \left(\frac{N_s}{N_p}\right)} \right) \quad (2)$$

where, $V_{th} = kT/q$, k is the Boltzmann constant, q is electron charge, and T is the cell temperature in Kelvin degrees.

3. Experimental Set up

All the experimental work for has been conducted at the National Institute of Solar Energy (NISE), Gurugram, Haryana, India.

3.1 PV Modules Used

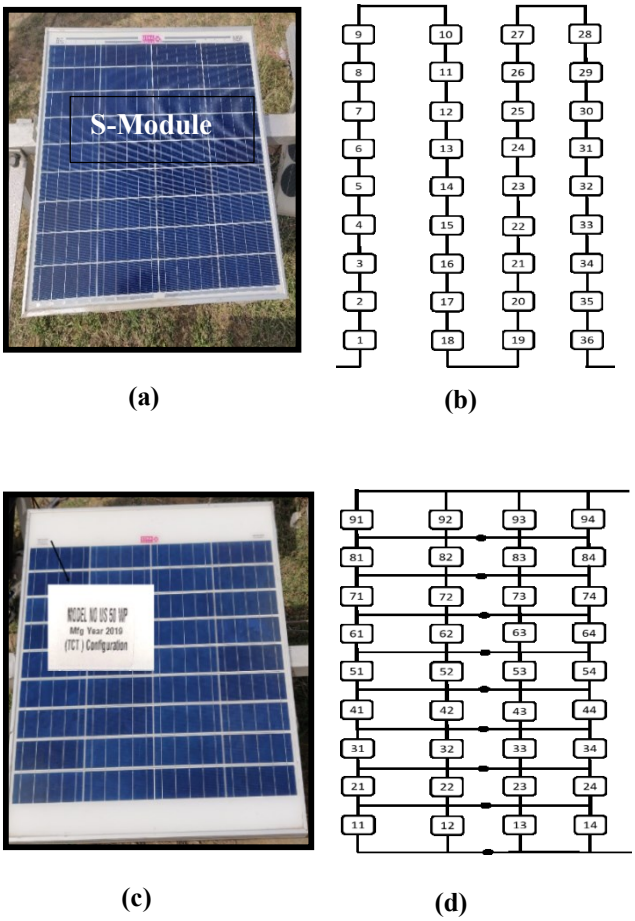

Fig. 2. Module and their interconnections: (a) S-module (b) cell interconnections of S-module (c) TCT-module (d) cell interconnections of TCT-module.

Poly-crystalline Si PV modules with series and total cross tied interconnection of cell has been used for this study. The modules have 9x4 architecture i.e., 36 solar cells arranged in 4 columns, each having 9 cells. The dimension of each solar cell is 2" x 6". The PV modules picture and their cell interconnection design is presented in Fig. 2. The obtained electrical parameters of both the module at standard test conditions (STC) of 1000 W/m^2 and 25°C is presented in Table.1.

3.2 Instrument used for the Measurement of PV Characteristics

The measurement of output characteristics of TCT and S module has been done using a solar simulator. It is a scientific equipment which mimics the natural sunlight in a controlled laboratory environment. It is a pivotal instrument in the field of photovoltaics. It is used for the indoor measurement of the electrical characteristics of PV cells and modules [35],[36]. The solar simulator used in this work for the characterisation of the module is Endeas QuickSun 700A sun simulator (Fig. 3).

Table 1. Electrical parameters of S-module and TCT-module at STC

Parameters	S-module	TCT-module
Maximum power rating [Wp]	49.8 Wp	46.0 Wp
Maximum power voltage (V_{mp})	18.6 V	4.35 V
Maximum power current (I_{mp})	2.67A	10.56 A
Open circuit voltage (V_{oc})	22.4 V	5.81 V
Short circuit current (I_{sc})	2. 83 A	11.48 A
No. of cells	36	36
Interconnection scheme of cells	Series	Total-cross-tied

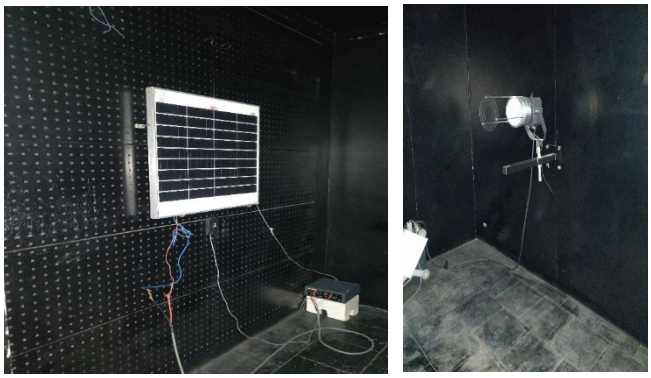

Fig. 3. Endeas QuickSun 700A solar simulator at NISE (a) TCT PV module placed in the testing chamber (b) Xenon lamp.

It is a large area class AAA solar simulator which measures the current-voltage characteristics of crystalline or thin film PV modules. It has the measurement or testing area of up to 160 cm x 220 cm. The light source used is the Xenon flash tube with AM1.5G filter. The irradiance level can be adjusted from 200-1200 W/m^2, with 1 W/m^2 resolution. The spectral match, non-uniformity of irradiance and temporal stability is in accordance with IEC60904-9. The measurement uncertainty is as per standard IEC60904-1. As per the manufacturer's specifications, the current and voltage measurement accuracy is ± 0.2%. The temperature and irradiance measurement accuracy are ± 1% and ± 3% respectively. The power reproducibility is +/- 0.25% [37].

3.3 Shading Scenarios Considered

Two progressive shading scenarios have been generated artificially which are based on the real-life shading conditions encountered by the roof-top PV installations:

Shading scenario 1: Shading due to cloud passage

Roof top installed PV modules are often encountered with shading due to cloud passage. The shading due to cloud passage considered in this study is shown in Fig. 4. The clouds have been considered to flow from left-top to right-bottom direction covering different percentage of total module area ranging from 2.7% to 47.2%. The output characteristics have been recorded at conditions of 800W/m^2 irradiance and 45°C module operating temperature. The irradiance of the cells under shading is 480 W/m^2, which is achieved by using a paper sheet of 48% transmissivity.

Shading scenario 2: Horizontal shading

The second scenario considered is based on the inter-row shading of PV modules commonly encountered in field conditions, as shown in Fig. 5. This is a self-shading of PV module, where the front PV module cast its shadow on the row of cells of PV module behind it. This type of shading commonly occurs when there is a limited space to install roof top PV array or when the space between rows of PV modules is not optimal. In this work, progression of the shadow is considered in the horizontal direction. The shading scenario has been categorized into twelve cases where the shadow progresses horizontally until it covers one entire row of the module. The schematic of the shadow progression is presented in Fig. 6. The output characteristics have been recorded at conditions of 1000W/m^2 irradiance and 25°C module operating temperature. The solar cells under shading do not receive any irradiance, which is achieved by using a thick black sheet of zero transmissivity.

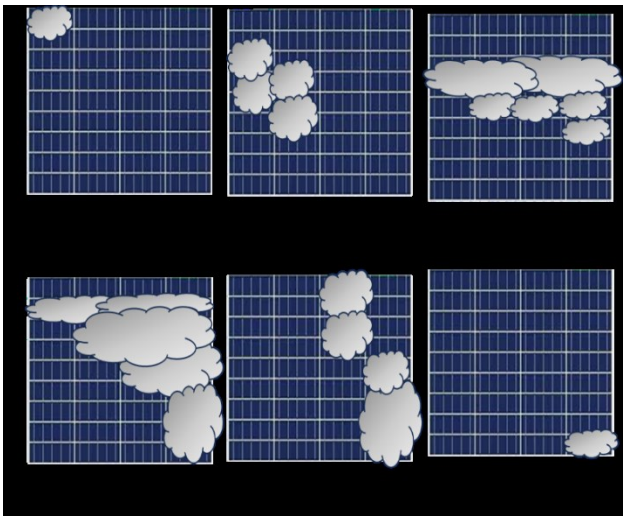

Fig. 4. Cloud passage shadow scenarios considered: (A) 4.2%, (B) 22.2%, (C) 33.3%, (D) 47.2%, (E) 25%, and (F) 2.7% of the PV module shaded.

Fig. 5. Inter-row or self-shading of PV module in field conditions (Picture source [38]).

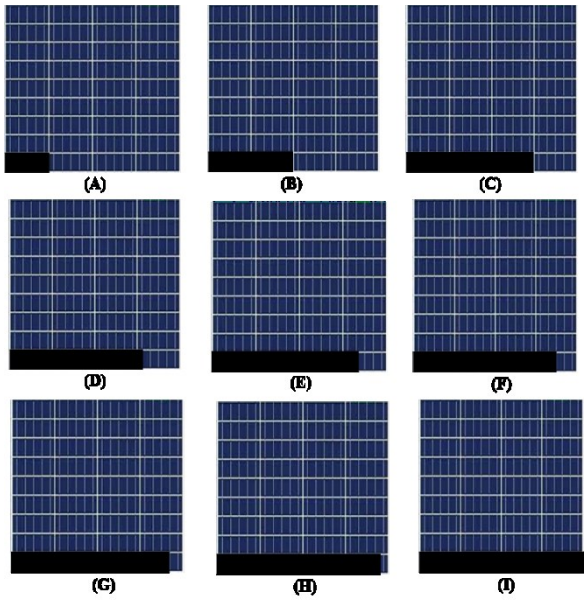

Fig. 6. Schematic of the shadow progression in horizontal direction (A) 25% (B) 50% (C) 75% (D) 77.5% (E) 82.5% (F) 87.5% (G) 92.5% (H) 97.5% (I) 100% of the row shaded.

4. Performance Assessment Parameters

The performance of both TCT and S configuration under PSCs has been assessed in terms of open circuit voltage (V_{oc}), short circuit current (I_{sc}), series resistance (R_s), maximum output power (P_{ms}), voltage at maximum power point (V_m), current at maximum power point (I_m), power loss due to shading (P_{LS}) and efficiency (η).

The power generated by the PV module under any particular shading case (P_{ms}) is the product of voltage and current at maximum power point.

$$P_{ms} = I_m \times V_m \tag{3}$$

The values of series resistances R_s for the modules are estimated from the slope of their I–V curve near $V=V_{oc}$ using Eq. (4) [39].

$$R_s \approx C_s \left(\frac{V_{oc}-V_m}{I_m}\right) \tag{4}$$

The values of coefficient $C_s = 0.34$ for multi-crystalline Si.

The PV power loss under any particular shading case is defined by Eq. (5)

$$P_{LS}\,(\%) = \frac{P_{max}-P_{ms}}{P_{max}} \times 100 \tag{5}$$

Where P_{max} is the maximum output power of the PV module under unshaded conditions.

Efficiency (η) of a PV module is the ratio of the electrical power output and the solar irradiance input over the device area and is given by Eq. (6)

$$\eta\ (\%) = \frac{V_{mp} \times I_{mp}}{G \times A} \times 100 \quad (6)$$

where 'G' is the input solar irradiance per unit area (W/m^2) and 'A' is the area of the PV array on which it falls.

5. Results and Discussion

5.1 For Shading due to the Cloud Passage

The obtained values of open circuit voltage, short circuit current, voltage at maximum power point, current at maximum power point, series resistance, maximum power and power loss and efficiency for both TCT and S configuration with cloud passage is presented in Table 2.

For shading case A when 4.2% of module area is covered by clouds, the power loss of TCT configuration is 28.3% while for S module it is 38.6%.

For shading case B where 22.2% of module area is covered by clouds, the power loss suffered by TCT configuration is 36.1% while for S module it is 46.4%. In going from case A to case B, the increase in power loss of both the configuration is 7.8% and efficiency decreases by 10.0%.

When clouds coverage increases to 33.3% i.e., shading case C, the power loss of TCT configuration is 46.7% while for S module it is 47.6%. In going from case B to case C, the increase in power loss of TCT configuration is 10.6% and efficiency decreases by 1.4%., while for S configuration the increase in power loss is only 1.2% and efficiency decreases by 0.1%.

For shading case D where 47.2% of module area is covered by clouds, the power loss suffered by TCT configuration is 43.3% while for S module it is 49.2%. It is interesting to note that while going from case C to case D, though the percentage of module area shaded by clouds increased from 33.3% to 47.2%, yet the power loss suffered by TCT configuration decreased by 3.4% and efficiency increased by 0.5%. For S configuration, power loss increased by 1.6% and efficiency decreases by 0.2%.

Under shading case E clouds start receding, shading 25.0% of the module area, the power loss suffered by TCT configuration is 33.7% while for S module it is 47.0%. In going from case D to case E, the decrease in power loss of TCT is 9.6% while for S configuration it is only 2.2%. Also, the efficiency of TCT and S configuration increases by 1.2% and 0.3% respectively as shading scenario changes from D to E.

For shading case F, when clouds are shading only 2.7% of the module area, the power loss suffered by TCT configuration is 27.4% while for S module it is 38.2%. In going from case E to case F, the decrease in power loss of TCT is 6.3% while for S configuration it is 8.8%. Also, the efficiency of TCT and S configuration increases by 0.8% and 1.2% respectively as shading scenario changes from E to F.

Table 2. Obtained results for S and TCT configuration under different cases of cloud shading

Cloud Shading Case A (4.2% module area shaded)								
Configuration	**V_{oc} (V)**	**I_{sc} (A)**	**V_m (V)**	**I_m (A)**	**R_s (Ω)**	**P_m (W)**	**PL (%)**	**Ƞ (%)**
TCT	5.21	9.05	3.81	8.66	0.055	33.0	28.3	9.3
S	20.9	2.39	19.2	1.59	0.364	30.6	38.6	8.6
Cloud Shading Case B (22.2% module area shaded)								
Configuration	**V_{oc} (V)**	**I_{sc} (A)**	**V_m (V)**	**I_m (A)**	**R_s (Ω)**	**P_m (W)**	**PL (%)**	**Ƞ (%)**
TCT	5.14	7.88	4.03	7.31	0.052	29.4	36.1	8.3
S	20.9	2.44	18.9	1.41	0.482	26.7	46.4	7.5
Cloud Shading Case C (33.3% module area shaded)								
Configuration	**V_{oc} (V)**	**I_{sc} (A)**	**V_m (V)**	**I_m (A)**	**R_s (Ω)**	**P_m (W)**	**PL (%)**	**Ƞ (%)**
TCT	5.10	5.99	4.28	5.71	0.049	24.5	46.7	6.9
S	20.7	1.5	17.85	1.46	0.664	26.1	47.6	7.4

Cloud Shading Case D (47.2% module area shaded)								
Configuration	**V_{oc} (V)**	**I_{sc} (A)**	**V_m (V)**	**I_m (A)**	**R_s (Ω)**	**P_m (W)**	**PL (%)**	**η (%)**
TCT	5.12	6.38	4.22	6.19	0.049	26.1	43.3	7.4
S	20.3	1.48	17.78	1.43	0.599	25.3	49.2	7.2
Cloud Shading Case E (25.0% module area shaded)								
Configuration	**V_{oc} (V)**	**I_{sc} (A)**	**V_m (V)**	**I_m (A)**	**R_s (Ω)**	**P_m (W)**	**PL (%)**	**η (%)**
TCT	5.19	8.52	3.93	7.77	0.055	30.5	33.7	8.6
S	20.98	2.4	18.67	1.41	0.557	26.4	47.0	7.5
Cloud Shading Case F (2.7% module area shaded)								
Configuration	**V_{oc} (V)**	**I_{sc} (A)**	**V_m (V)**	**I_m (A)**	**R_s (Ω)**	**P_m (W)**	**PL (%)**	**η (%)**
TCT	5.23	9.03	3.87	8.63	0.054	33.4	27.4	9.4
S	20.48	2.39	18.86	1.64	0.336	30.8	38.2	8.7

5.2 For Inter-Row Shading

The obtained values of open circuit voltage, short circuit current, voltage at maximum power point, current at maximum power point, series resistance, maximum power and power loss and efficiency for both TCT and S configuration with shadow progression in horizontal direction is presented in Table 3.

For case A, where shadow covers 25% of the row, the power loss suffered by TCT configuration is 10.7%. The S configuration suffers a huge power loss of 50.6% with just one cell shading. The efficiency decreased by 10.6% for TCT and 50.4% for S configuration w.r.t the efficiency under unshaded condition

Table 3. Obtained results for S and TCT configuration under different cases of horizontal shading

Horizontal Shading Case A (25.0% row shaded)								
Configuration	**V_{oc} (V)**	**I_{sc} (A)**	**V_m (V)**	**I_m (A)**	**R_s (o)**	**P_m (W)**	**PL (%)**	**η (%)**
TCT	5.78	9.25	4.59	8.94	0.045	41.1	10.7	9.3
S	22.32	2.83	9.01	2.73	1.657	24.6	50.6	5.6
Horizontal Shading Case B (50.0% row shaded)								
Configuration	**V_{oc} (V)**	**I_{sc} (A)**	**V_m (V)**	**I_m (A)**	**R_s (o)**	**P_m (W)**	**PL (%)**	**η (%)**
TCT	5.73	6.31	4.89	6.11	0.047	29.9	35.0	6.8
S	22.31	2.83	9.01	2.73	1.659	24.6	50.8	5.5
Horizontal Shading Case C (75.0% row shaded)								
Configuration	**V_{oc} (V)**	**I_{sc} (A)**	**V_m (V)**	**I_m (A)**	**R_s (o)**	**P_m (W)**	**PL (%)**	**η (%)**
TCT	5.66	3.40	5.11	3.26	0.057	16.6	63.9	3.8
S		-	-	-	-	0	100	0
Horizontal Shading Case D (77.5% row shaded)								
Configuration	**V_{oc} (V)**	**I_{sc} (A)**	**V_m (V)**	**I_m (A)**	**R_s (o)**	**P_m (W)**	**PL (%)**	**η (%)**
TCT	5.64	3.08	5.13	2.98	0.058	15.3	66.7	3.5
S		-	-	-	-	0	100	0
Horizontal Shading Case E (82.5% row shaded)								

Configuration	V_{oc} (V)	I_{sc} (A)	V_m (V)	I_m (A)	R_s (o)	P_m (W)	PL (%)	η (%)
TCT	5.62	2.50	5.16	2.41	0.065	12.5	72.8	2.8
S		-	-	-	-	0	100	0
Horizontal Shading Case F (87.5% row shaded)								
Configuration	**V_{oc} (V)**	**I_{sc} (A)**	**V_m (V)**	**I_m (A)**	**R_s (o)**	**P_m (W)**	**PL (%)**	**η (%)**
TCT	5.61	1.89	5.19	1.82	0.078	9.4	79.6	2.1
S		-	-	-	-	0	100	0
Horizontal Shading Case G (92.5% row shaded)								
Configuration	**V_{oc} (V)**	**I_{sc} (A)**	**V_m (V)**	**I_m (A)**	**R_s (o)**	**P_m (W)**	**PL (%)**	**η (%)**
TCT	5.58	1.36	5.19	1.29	0.103	6.7	85.4	1.5
S		-	-	-	-	0	100	0
Horizontal Shading Case H (97.5% row shaded)								
Configuration	**V_{oc} (V)**	**I_{sc} (A)**	**V_m (V)**	**I_m (A)**	**R_s (o)**	**P_m (W)**	**PL (%)**	**η (%)**
TCT	5.56	0.77	5.17	0.71	0.187	3.6	92.2	0.8
S		-	-	-	-	0	100	0
Horizontal Shading Case I (100% row shaded)								
Configuration	**V_{oc} (V)**	**I_{sc} (A)**	**V_m (V)**	**I_m (A)**	**R_s (o)**	**P_m (W)**	**PL (%)**	**η (%)**
TCT	5.56	0.44	5.12	0.39	0.384	0	100	0
S		-	-	-	-	0	100	0

For shading case B where 50% of the row is shaded, the power loss suffered by TCT configuration is 35.0% while for S module it is 50.8%, approximately same as previous case. In going from case A to case B, the increase in power loss of TCT configuration is 24.3%, while for S configuration it is nearly 0%. The efficiency decreases by 2.5% for TCT and 0.1% for S configuration w.r.t the efficiency obtained under shading case A.

For shading case C where 75% of the row is shaded, the power loss suffered by TCT configuration is 63.9% while for S module it is 100%. In going from case B to case C, the increase in power loss of TCT configuration is 28.9%, while for S configuration it is nearly 50%. The decrease in efficiency of TCT is 3.0% and for S configuration it is 5.5% w.r.t the efficiency obtained under shading case B.

For shading case D where 77.5% of the row is shaded, the power loss suffered by TCT configuration is 66.7% while for S module it is again100%. In going from case C to case D, the increase in power loss of TCT configuration is 2.8%, and the decrease in efficiency is 0.3%.

For shading case E where 82.5% of the row is shaded, the power loss suffered by TCT configuration is 72.8% while for S module it is again100%. In going from case D to case E, the power loss of TCT configuration increases by 6.1%, and the efficiency decreases by 0.7%.

For shading case F where 87.5% of the row is shaded, the power loss of TCT configuration is 79.6% while for S module it is again100%. In going from case E to case F, the increase in power loss of TCT configuration is 6.8%, and the decrease in efficiency is 0.7%.

For shading case G where 92.5% of the row is shaded, the power loss suffered by TCT configuration is 85.4% while for S module it is again100%. In going from case F to case G, the increase in power loss of TCT configuration is 5.8%, and the efficiency decreases by 0.6%.

For shading case H where 97.5% of the row is shaded, the power loss suffered by TCT configuration is 92.2% while for S module it is again100%. In going from case G to case H, the increase in power loss of TCT configuration is 6.8%, and the efficiency decreases by 0.7%.

For shading case I where 100% of the row is shaded, the power loss suffered by TCT configuration is100%, while for S module it is also100%. In going from case H to case I, the increase in power loss of TCT configuration is 7.8%, and the efficiency decreases by 0.8 %.

The above results clearly demonstrates that when the shadow progresses horizontally, the power loss of TCT configuration increases with increase in shaded area. Even when a fraction of a single cell is shaded, the performance of TCT configuration gets impacted. However, a TCT

configured module can generate power even when 97.5% of the row is shaded with 100% intensity. On the other hand, a S-configured module stops generating any power as soon as the two PV cells belonging to two different strings are shaded with 100% (case C and onwards). But, if the two cells of the same string are shaded with 100% intensity, S module can generate nearly 50% power, which in case of TCT is 65%.

5.3 Pattern of power loss suffered by TCT configuration under both the shading scenarios

The power loss suffered by TCT configuration under different cases of cloud and horizontal shading is presented in Fig. 7.

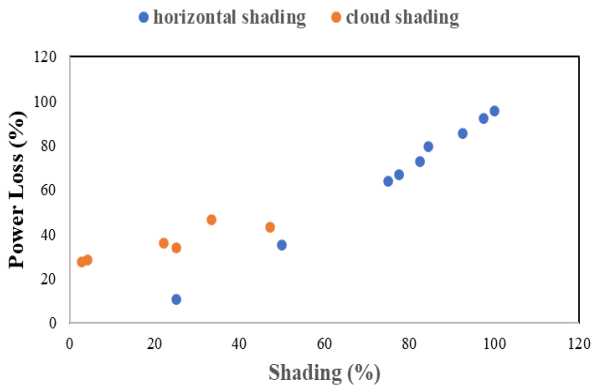

Fig. 7. Pattern of power loss suffered by TCT configuration under different cases of cloud and horizontal shading.

In case of progressing horizontal shading or row shading, the power loss and shading area (%) exhibits a linear relationship. However, in case of cloud shading it is clear that increasing the shaded area doesn't necessarily means increase in power loss. TCT configuration suffers lower power loss even if the shaded area of the module is more, as demonstrated in case D w.r.t C, and case E w.r.t B. This is owing to the cross tied interconnection scheme, which displays lower power loss if less rows are shaded even when area shaded is more. TCT displays higher power loss only if more rows are shaded even when shaded area of the module is less.

6. Conclusion

In this paper, performance of TCT and S PV configuration have been studied experimentally under two realistic scenarios of progressing PSCs. These shading conditions are based on the shading due passage of cloud and self-shading in roof top installed PV system. Values of open circuit voltage, short circuit current, voltage at maximum power point, current at maximum power point, series resistance, maximum power, power loss and efficiency for both TCT and S module with shadow progression under both the shading scenario has been recorded. In case of progressing horizontal row shading with constant shading intensity , the power loss (%) exhibits a linear relationship with the shading area. However, in case of cloud shading, an increase in the shaded area doesn't necessarily means increase in power loss. Even when the shaded area increases, the power loss can decrease in case of TCT configuration. This is contrary to S configuration where the power loss increases as the shading area increases. However, in general, TCT suffer less power loss than S configuration under varying PSCs.

Since the shape of the shadow changes continuously in real life, the insight presented in this paper are of significance in understanding the behaviour of TCT configuration over a long period of time under PSCs. The results of this study are also very significant especially for rooftop PV arrays in congested urban environment where it is highly probable that installed PV array is partially shaded for large number of days in a year.

Future scope of the work includes long-term performance of roof-top installed TCT PV array configuration under real dynamic shadow conditions.

Acknowledgement

The author is grateful to Dr. Chandan Banerjee at National Institute of Solar Energy (NISE), Gurugram, under Ministry of New and Renewable Energy (MNRE), Government of India, India for allowing to use the facilities for conducting this experimental study. My sincere thanks are due to Dr. Birinchi Bora and the staff at NISE for their support during this research work.

Funding

This research did not receive any specific grant from funding agencies in the public, commercial, or not-for-profit sectors.

References

[1] "Renewable capacity statistics 2021," IRENA 2021.

[2] "Future of solar photovoltaic: Deployment, investment, technology, grid integration and socio-economic aspects," IRENA, November 2019.

[3] A. Kumar Behura, A. Kumar, D. Kumar Rajak, C. I. Pruncu, and L. Lamberti, "Towards better performances for a novel rooftop solar PV system,"' Sol. Energy, vol. 216, pp. 518-529, Mar. 2021.

[4] R. J. Mustafa, M. R. Gomaa, M. Al-Dhaifallah, and H. Rezk, "Environmental impacts on the performance of solar photovoltaic systems,"' Sustainability, vol. 12, no. 2, p. 608, Jan. 2020.

[5] P. R. Satpathy, T. S. Babu, S. K. Shanmugam, L. N. Popavath and H. H. Alhelou, "Impact of uneven shading by neighboring buildings and clouds on the conventional and hybrid configurations of roof-top PV arrays," in IEEE Access, vol. 9, pp. 139059-139073, 2021, doi: 10.1109/ACCESS.2021.3118357.

[6] K. Lappalainen and S. Valkealahti, "Output power variation of different PV array configurations during

irradiance transitions caused by moving clouds," Applied Energy, vol. 190, 2017, doi: 10.1016/j.apenergy.2017.01.013.

[7] S. Vijayalekshmy, G. R. Bindu and S. R. Iyer, "Estimation of power losses in photovoltaic array configurations under moving cloud conditions," 2014 Fourth International Conference on Advances in Computing and Communications, Cochin, India, 2014, pp. 366-369, doi: 10.1109/ICACC.2014.91.

[8] K. Brecl and M. Topič, "Self-shading losses of fixed free-standing PV arrays," Renew Energy, vol. 36, no. 11, pp. 3211–3216, Nov. 2011, doi: 10.1016/j.renene.2011.03.011.

[9] K. A. K. Niazi, W. Akhtar, H. A. Khan, Y. Yang, and S. Athar, "Hotspot diagnosis for solar photovoltaic modules using a naive Bayes classifier," Sol. Energy, vol. 190, pp. 34_43, Sep. 2019.

[10] S. Hadji, L. Larbi, A. Belkaid, I. Colak and R. Bayindir, "Global optimum operating point tracker of PV system, under partial shading, using parallel searching," 2022 10th International Conference on Smart Grid (icSmartGrid), Istanbul, Turkey, 2022, pp. 227-230, doi: 10.1109/icSmartGrid55722.2022.9848552.

[11] N. Akoubi, "Combination of artificial neural network-based approaches to control a grid-connected photovoltaic source under partial shading condition," International Journal of Renewable Energy Research, Vol. 13, no.2, pp 778-789, June 2023.

[12] H. Oufettoul, S. Motahhir, I. A. Abdelmoula, G. Aniba, W. Issa and O. Mahir, "Optimum MPPT technique for reconfiguring the photovoltaic array under partial shading failure," 2023 12th International Conference on Renewable Energy Research and Applications (ICRERA), Oshawa, Canada, 2023, pp. 331-338, doi: 10.1109/ICRERA59003.2023.10269423.

[13] H. Karmouni et al., "A Novel MPPT Algorithm based on Aquila Optimizer under PSC and Implementation using Raspberry," 2022 11th International Conference on Renewable Energy Research and Application (ICRERA), Istanbul, Turkey, 2022, pp. 446-451, doi: 10.1109/ICRERA55966.2022.9922834.

[14] A. F. Mirza, M. Mansoor, Q. Ling, B. Yin, and M. Y. Javed, "A salp-swarm optimization based MPPT technique for harvesting maximum energy from PV systems under partial shading conditions," Energy Convers. Manage., vol. 209, Apr. 2020, Art. no. 112625.

[15] W. A. Abri, R. A. Abri, H. Yousef and A. Al-Hinai, "A global MPPT based on bald eagle search technique for PV system operating under partial shading conditions," 2022 10th International Conference on Smart Grid (icSmartGrid), Istanbul, Turkey, 2022, pp. 325-332, doi: 10.1109/icSmartGrid55722.2022.9848561.

[16] O. Guenounou, A. Belkaid, I. Colak, B. Dahhou and F. Chabour, "Optimization of fuzzy logic controller based maximum power point tracking using hierarchical genetic algorithms," 2021 9th International Conference on Smart Grid (icSmartGrid), Setubal, Portugal, 2021, pp. 207-211, doi: 10.1109/icSmartGrid52357.2021.9551249.

[17] F. Belhachat and C. Larbes, "PV array reconfiguration techniques for maximum power optimization under partial shading conditions: A review," Solar Energy, vol. 230, pp. 558–582, Dec. 01, 2021. doi: 10.1016/j.solener.2021.09.089.

[18] G. Sai Krishna and T. Moger, "Reconfiguration strategies for reducing partial shading effects in photovoltaic arrays: State of the art," Sol. Energy, vol. 182, pp. 429_452, Apr. 2019.

[19] S. Vunnam, M. VanithaSri, R. Alla, "An optimal triple-series parallel-ladder topology for maximum power harvesting under partial shading conditions," International Journal of Renewable Energy Research, Vol. 13, no.2, pp 888-898, June 2023.

[20] N. Agrawal, B. Bora, A. Kapoor, Experimental investigations of fault tolerance due to shading in photovoltaic modules with different interconnected solar cell networks. Solar Energy 2020, 211, 1239-1254.

[21] N. Agrawal, B. Bora, S. Rai, A. Kapoor, M. Gupta, "Performance enhancement by novel hybrid PV array without and with bypass diode under partial shaded conditions: an experimental study", International Journal of Renewable Energy Research 2021, 11, 1880-1891.

[22] O. Bingöl and B. Özkaya, "Analysis and comparison of different PV array configurations under partial shading conditions," Solar Energy, vol. 160, pp. 336–343, Jan. 2018, doi: 10.1016/j.solener.2017.12.004.

[23] S. R. Pendem and S. Mikkili, "Modelling and performance assessment of PV array topologies under partial shading conditions to mitigate the mismatching power losses," Solar Energy, vol. 160, pp. 303–321, Jan. 20 18, doi: 10.1016/j.solener.2017.12.010.

[24] S. Bana and R. P. Saini, "Experimental investigation on power output of different photovoltaic array configurations under uniform and partial shading

scenarios," Energy, vol. 127, pp. 438–453, 2017, doi: 10.1016/j.energy.2017.03.139.

[25] F. Belhachat and C. Larbes, "Modeling, analysis and comparison of solar photovoltaic array configurations under partial shading conditions," Solar Energy, vol. 120, pp. 399–418, Oct. 2015, doi: 10.1016/j.solener.2015.07.039.

[26] B. I. Rani, G. S. Ilango, and C. Nagamani, "Enhanced power generation from PV array under partial shading conditions by shade dispersion using Su Do Ku configuration,", vol. 4, no. 3, pp. 594–601, 2013, doi: 10.1109/TSTE.2012.2230033.

[27] G. Sagar, D. Pathak, P. Gaur, and V. Jain, "A Su Do Ku puzzle based shade dispersion for maximum power enhancement of partially shaded hybrid bridge-link-total-cross-tied PV array," Solar Energy, vol. 204, pp. 161–180, Jul. 2020, doi: 10.1016/j.solener.2020.04.054.

[28] P. Srinivasa Rao, P. Dinesh, G. Saravana Ilango, and C. Nagamani, "Optimal Su-Do-Ku based interconnection scheme for increased power output from PV array under partial shading conditions," Frontiers in Energy, vol. 9, no. 2, pp. 199–210, 2015, doi: 10.1007/s11708-015-0350-1.

[29] M. Horoufiany and R. Ghandehari, "Optimization of the Sudoku based reconfiguration technique for PV arrays power enhancement under mutual shading conditions," Solar Energy, vol. 159, pp. 1037–1046, Jan. 2018, doi: 10.1016/J.SOLENER.2017.05.059.

[30] A. S. Yadav, R. K. Pachauri, Y. K. Chauhan, S. Choudhury, and R. Singh, "Performance enhancement of partially shaded PV array using novel shade dispersion effect on magic-square puzzle configuration," Solar Energy, vol. 144, pp. 780–797, 2017, doi: 10.1016/j.solener.2017.01.011.

[31] B. Dhanalakshmi and N. Rajasekar, "Dominance square based array reconfiguration scheme for power loss reduction in solar Photovoltaic (PV) systems," Energy conversion and Management, vol. 156, pp. 84–102, Jan. 2018, doi: 10.1016/J.ENCONMAN.2017.10.080.

[32] M. S. S. Nihanth, J. P. Ram, D. S. Pillai, A. M. Y. M. Ghias, A. Garg, and N. Rajasekar, "Enhanced power production in PV arrays using a new skyscraper puzzle based one-time reconfiguration procedure under partial shade conditions (PSCs)," Solar Energy, vol. 194, pp. 209–224, Dec. 2019, doi: 10.1016/j.solener.2019.10.020.

[33] M. G. Villalva, J. R. Gazoli, and E. R. Filho, "Comprehensive approach to modeling and simulation of photovoltaic arrays," IEEE Trans Power Electron, vol. 24, no. 5, pp. 1198–1208, 2009, doi: 10.1109/TPEL.2009.2013862.

[34] M. Kermadi, V. J. Chin, S. Mekhilef, and Z. Salam, "A fast and accurate generalized analytical approach for PV arrays modeling under partial shading conditions," Solar Energy, vol. 208, pp. 753–765, Sep. 2020, doi: 10.1016/J.SOLENER.2020.07.077.

[35] R. V. Parupudi, H. Singh, and M. Kolokotroni, "Sun Simulator for Indoor Performance assessment of Solar Photovoltaic Cells," Energy Procedia, vol. 161, pp. 376–384, Mar. 2019, doi: 10.1016/j.egypro.2019.02.102.

[36] D. Bari et al., "Reliability study of dye-sensitized solar cells by means of solar simulator and white LED," Microelectronics Reliability, vol. 52, no. 9, pp. 2495–2499, 2012, doi: https://doi.org/10.1016/j.microrel.2012.06.061.

[37] https://916.icstm.ro/sites/916.icstm.ro/files/file/QuickSun700A.pdf

[38] "Partial Shading in Monolithic Thin Film PV Modules: Analysis and Design." https://www.energy.gov/sites/default/files/2014/01/f7/pvmrw13_ps1_purdue_dongaonkar.pdf

[39] A. P. Dobos, "An improved coefficient calculator for the california energy commission 6 parameter photovoltaic module model," Journal of Solar Energy Engineering, Transactions of the ASME, vol. 134, no. 2, 2012, doi: 10.1115/1.4005759.